Inorganic Chemistry

Article

pubs.acs.org/IC

α-$ScVSe_2O_8$, β-$ScVSe_2O_8$, and $ScVTe_2O_8$: New Quaternary Mixed Metal Oxides Composed of Only Second-Order Jahn–Teller Distortive Cations

Yeong Hun Kim, Dong Woo Lee, and Kang Min Ok*

Department of Chemistry, Chung-Ang University, 221 Heukseok-dong, Dongjak-gu, Seoul 156-756, Republic of Korea

Supporting Information

ABSTRACT: Three new quaternary scandium vanadium selenium/tellurium oxides, α-$ScVSe_2O_8$, β-$ScVSe_2O_8$, and $ScVTe_2O_8$ have been synthesized through hydrothermal and standard solid-state reactions. Although all three reported materials are stoichiometrically similar, they exhibit different crystal structures: α-$ScVSe_2O_8$ has a three-dimensional framework structure consisting of ScO_6, VO_6, and SeO_3 groups. β-$ScVSe_2O_8$ reveals another three-dimensional framework composed of ScO_7, VO_5, and SeO_3 polyhedra. $ScVTe_2O_8$ shows a layered structure with ScO_6, VO_4, and TeO_4 polyhedra. Interestingly, the constituent cations, that is, Sc^{3+}, V^{5+}, Se^{4+}, and Te^{4+} are all in a distorted coordination environment attributable to second-order Jahn–Teller (SOJT) effects. Complete characterizations including infrared spectroscopy, elemental analyses, thermal analyses, dipole moment calculation, and the magnitudes of out-of-center distortions for the compounds are reported. Transformation reactions suggest that α-$ScVSe_2O_8$ may change to β-$ScVSe_2O_8$, and then to $Sc_2(SeO_3)_3{\cdot}H_2O$ under hydrothermal conditions.

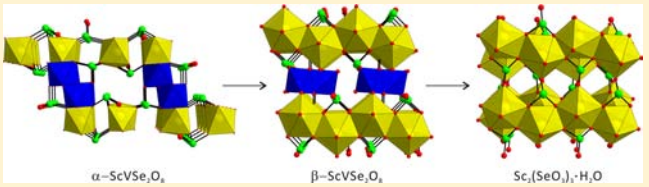

INTRODUCTION

A variety of technologically important physical properties such as ferroelectricity, pyroelectricity, piezoelectricity, and second-harmonic generation (SHG) are normally observed in materials crystallizing in macroscopic noncentrosymmetric (NCS) classes.[1] Thus, synthetic chemists have been combining cations with asymmetric coordination environments as important building units to discover new functional NCS materials. With oxide materials, the acentric coordination moieties are generally found in two families of cations, that is, octahedrally coordinated d^0 transition metal cations (Ti^{4+}, V^{5+}, Mo^{6+}, etc.) and lone pair cations (Sn^{2+}, Sb^{3+}, Te^{4+}, etc.). For both families of cations, the observed distortive coordination environments are considered to be the result of electronic second-order Jahn–Teller (SOJT) effects.[2] The SOJT effects for the octahedrally coordinated d^0 transition metal cations normally occur when the empty d-orbitals of the metal mix with the filled p-orbitals of the ligands. The octahedral distortions often occur along one of three directions: local C_2 direction toward an edge, local C_3 direction toward a face, or local C_4 direction toward a corner.[3] The situation with the lone pair cations is more complex: the mixing of the metal s- and p-orbitals had been considered as the main reason for the cationic distortion and polarization.[4] Recently, however, many researchers have argued that the strong interaction of the s- and p-orbitals of cation with the anion p-orbitals is critical for lone pair formation.[5] Anyhow, in both instances, the structural consequences from the asymmetric coordination environment arising from the SOJT effects are profound. Moreover, materials containing both d^0 transition metal cations and lone pair cations can reveal a rich structural chemistry with a great deal of framework flexibilities.[6] With these ideas in mind, we investigated the Sc^{3+}–V^{5+}–Q^{4+} (Q = Se or Te)–oxide system. Thus far, several quaternary vanadium selenite/tellurite materials containing alkali metals,[7] alkaline-earth metals,[8] and transition metals[9] have been reported. A few stoichiometrically similar phases, $M^{3+}VQ_2O_8$ (M = Bi, Eu, Gd, Tb, and In), also have been discovered, where $InVSe_2O_8$ crystallizes in NCS framework structures with SHG efficiency of 30 times that of α-SiO_2.[10] Here we report three new quaternary scandium vanadium selenium/tellurium oxides, α-$ScVSe_2O_8$, β-$ScVSe_2O_8$, and $ScVTe_2O_8$, in which all of the constituent cations are SOJT distortive. Complete structural analyses, infrared spectra, elemental analyses, thermal analyses, dipole moment calculations, and the magnitudes of out-of-center distortions for the reported materials are presented. In addition, transformation reactions of $ScVSe_2O_8$ phases under hydrothermal conditions will be discussed.

EXPERIMENTAL SECTION

Reagents. Sc_2O_3 (Alfa Aesar, 99.4%), V_2O_5 (Junsei, 99%), SeO_2 (Aldrich, 99.8%), and TeO_2 (Alfa Aesar, 98%) were used as received.

Synthesis. Crystals of α-$ScVSe_2O_8$ were prepared by hydrothermal reactions. A 0.069 g portion (5.00×10^{-4} mol) of Sc_2O_3, 0.091 g (5.00×10^{-4} mol) of V_2O_5, 0.444 g (4.00×10^{-3} mol) of SeO_2, and 5 mL of deionized water were combined. The reaction mixture was loaded into a 23 mL Teflon-lined stainless steel autoclave. The autoclave was subsequently sealed and gradually heated to 230 °C, held for 4 days, and cooled to room temperature at a rate of 6 °C h^{-1}. After cooling, the autoclave was opened and the product was recovered by filtration and washed with distilled water. Green crystals of α-$ScVSe_2O_8$ were obtained

Received: July 10, 2013
Published: September 11, 2013

in 24% yield based on Sc_2O_3. Crystals of β-$ScVSe_2O_8$ and $ScVTe_2O_8$ were prepared by standard solid-state reactions. For single crystals of β-$ScVSe_2O_8$, 0.138 g (1.00×10^{-3} mol) of Sc_2O_3, 0.091 g (5.00×10^{-4} mol) of V_2O_5, and 0.444 g (4.00×10^{-3} mol) of SeO_2 were combined. For crystal growth of $ScVTe_2O_8$, 0.069 g (5.00×10^{-4} mol) of Sc_2O_3, 0.091 g (5.00×10^{-4} mol) of V_2O_5, and 0.479 g (3.00×10^{-3} mol) of TeO_2 were combined. Each reaction mixture was thoroughly ground with agate mortars and pestles. The respective reaction mixtures were then pressed into pellets and introduced into fused silica tubes that were subsequently evacuated and sealed. Each tube was gradually heated to 350 °C for 5 h, 450 °C (700 °C for $ScVTe_2O_8$) for 48 h, and cooled at a rate of 6 °C h^{-1} to room temperature. While colorless crystals of $ScVTe_2O_8$ were successfully obtained from the synthesis reaction, light yellow crystals of β-$ScVSe_2O_8$ were isolated from the product mixture containing polycrystalline α-$ScVSe_2O_8$ and some unknown amorphous phases. After determining the crystal structures, pure bulk polycrystalline samples of α-$ScVSe_2O_8$ and $ScVTe_2O_8$ were synthesized through similar standard solid-state reactions: stoichiometric amounts of starting materials, Sc_2O_3, V_2O_5, and SeO_2 (or TeO_2) were thoroughly mixed and introduced into a fused silica tube, and the tube was evacuated and sealed. Each tube was gradually heated to 450 °C for 36 h (450, 500, 600, and 650 °C for 48 h for $ScVTe_2O_8$) with three intermediate regrindings. Although several attempts have been made to prepare pure samples of β-$ScVSe_2O_8$, α-$ScVSe_2O_8$ was always accompanied. Thus, β-$ScVSe_2O_8$ was manually isolated from the product mixture based on the crystal color and morphology for further characterization. The powder X-ray diffraction (XRD) patterns on the resultant products were in good agreements with the generated patterns from the single-crystal data (see the Supporting Information).

Single Crystal XRD. The crystal structures of α-$ScVSe_2O_8$, β-$ScVSe_2O_8$, and $ScVTe_2O_8$ were determined by standard crystallographic methods. A green rod ($0.012 \times 0.015 \times 0.032$ mm^3) for α-$ScVSe_2O_8$, a light yellow block ($0.021 \times 0.028 \times 0.037$ mm^3) for β-$ScVSe_2O_8$, and a colorless plate ($0.023 \times 0.045 \times 0.016$ mm^3) for $ScVTe_2O_8$ were used for single crystal data analyses. All of the data were collected using a Bruker SMART BREEZE diffractometer equipped with a 1K CCD area detector using graphite monochromated Mo Kα radiation at room temperature. A hemisphere of data was collected using a narrow-frame method with scan widths of 0.30° in ω, and an exposure time of 5 s/frame. The first 50 frames were remeasured at the end of the data collection to monitor instrument and crystal stability. The maximum correction applied to the intensities was <1%. The data were integrated using the SAINT program,[11] with the intensities corrected for Lorentz factor, polarization, air absorption, and absorption attributable to the variation in the path length through the detector faceplate. A semiempirical absorption correction was made on the hemisphere of data with the SADABS program.[12] The data were solved and refined using SHELXS-97[13] and SHELXL-97,[14] respectively. All calculations were performed using the WinGX-98 crystallographic software package.[15] Crystallographic data and selected bond distances for the reported material are given in Tables 1 and 2.

Powder XRD. The powder XRD data were collected on a Bruker D8-Advance diffractometer using Cu Kα radiation at room temperature with 40 kV and 40 mA. The polycrystalline samples were mounted on sample holders and scanned in the 2θ range 5−70° with a step size of 0.02°, and a step time of 0.2 s. The experimental powder XRD patterns are in good agreement with those calculated data from the single-crystal models.

Infrared Spectroscopy. Infrared spectra were recorded on a Varian 1000 FT-IR spectrometer in the 400−4000 cm^{-1} range, with the sample embedded in a KBr matrix.

Thermogravimetric Analysis. Thermogravimetric analysis was performed on a Setaram LABSYS TG-DTA/DSC Thermogravimetric Analyzer. The polycrystalline samples were contained within alumina crucibles and heated at a rate of 10 °C min^{-1} from room temperature to 1000 °C under flowing argon.

Scanning Electron Microscopy/Energy Dispersive Analysis by X-ray (SEM/EDAX). SEM/EDAX has been performed using a Hitachi S-3400N/Horiba Energy EX-250 instruments. EDAX for α-$ScVSe_2O_8$, β-$ScVSe_2O_8$, and $ScVTe_2O_8$ exhibit Sc/V/Se (or Te) ratios of 1.1:1.0:1.9, 0.9:1.0:2.0, and 0.8:1.0:2.1, respectively.

Table 1. Crystallographic Data for α-$ScVSe_2O_8$, β-$ScVSe_2O_8$, and $ScVTe_2O_8$

formula	$ScVSe_2O_8$	$ScVSe_2O_8$	$ScVTe_2O_8$
fw	381.82	381.82	479.10
space group	$P2_1/n$ (No. 14)	$P2_1/c$ (No. 14)	$P2_1/n$ (No. 14)
a (Å)	8.96460(10)	6.59040(10)	7.9774(2)
b (Å)	5.12600(10)	15.9098(3)	5.08710(10)
c (Å)	14.4802(2)	6.63740(10)	16.5654(4)
β (deg)	104.5740(10)	92.2790(10)	93.400(2)
V (Å^3)	570.09(10)	695.39(2)	671.07(3)
Z	4	4	4
T (K)	298.0(2)	298.0(2)	298.0(2)
λ (Å)	0.71073	0.71073	0.71073
ρ_{calcd} (g cm^{-3})	3.938	3.647	4.742
μ (mm^{-1})	13.814	12.793	10.932
$R(F)^a$	0.0200	0.0320	0.0413
$R_w(F_o^2)^b$	0.0434	0.0427	0.1064

$^aR(F) = \sum||F_o| - |F_c||/\sum|F_o|$. $^bR_w(F_o^2) = \{\sum[w(F_o^2 - F_c^2)^2]/\sum[w(F_o^2)^2]\}^{1/2}$.

RESULTS AND DISCUSSION

Structures. *α-$ScVSe_2O_8$.* α-$ScVSe_2O_8$ is a new quaternary Sc^{3+}−V^{5+}−Se^{4+}−oxide containing ScO_6, VO_6, and SeO_3 groups. The Sc^{3+} cations are in distorted octahedral coordination environment, linked to six oxygen atoms. The Sc−O bond distances range from 1.993(3) to 2.198(2) Å and the O−Sc−O bond angles range from 71.72(9) to 174.44(10)°. The V^{5+} cations are also in severely distorted octahedral coordination environment with six oxygen atoms. Specifically, the unique V^{5+} cation distorts toward an edge of the VO_6 octahedron (local C_2 direction), which results in two short (1.636(2) and 1.642(3) Å), two intermediate (1.933(2) and 2.005(2) Å), and two long (2.145(2) and 2.249(2) Å) V−O bond lengths. As expected from the distorted coordination environment, the observed O−V−O angles range from 75.53(9) to 172.24(12)°. The two unique Se^{4+} cations are connected to three oxygen atoms in asymmetric trigonal pyramidal coordination environments attributable to the stereoactive lone pair. The Se−O bond lengths and the O−Se−O bond angles range 1.665(2)−1.753(2) Å and 97.46(11)−104.15(11)°, respectively.

As can be seen in Figure 1a, two VO_6 octahedra share their edges through O(7) and form V_2O_{10} dimers. Then, ScO_6 octahedra share their edges through O(1) and O(6), and corners through O(8) with V_2O_{10} dimers, which generates infinite bands along the [010] direction (see Figure 1b). Six membered rings are observed from the unidimensional bands. A layered structure is obtained in the *ab*-plane once the $Se(2)O_3$ groups are linked to the bands, in which the $Se(2)O_3$ groups serve as interband linkers (see Figure 1c and d). Furthermore, the $Se(1)^{4+}$ cations connect the layers, bonding to oxygen atoms in adjacent layers along the [001] direction and form a three-dimensional framework structure. As can be seen in Figure 1e, small four-membered ring (4-MR) channels and large eight-membered ring (8-MR) channels that are running down the [010] direction are observed in the *ac*-plane. Within the 8-MR channels, lone pairs on Se^{4+} cations point in the [101] and [−10−1] directions. In connectivity terms, the structure of α-$ScVSe_2O_8$ may be described as a neutral framework of $\{[ScO_{4/2}O_{2/3}]^{-2.333}\ [VO_{4/2}O_{2/3}]^{-0.333}\ 2[SeO_{2/2}O_{1/3}]^{+1.333}\}^0$. Bond valence calculations[16] for the Sc^{3+}, V^{5+}, Se^{4+}, and O^{2-} result in values of 3.08, 5.09, 4.01−4.11, and 1.85−2.14, respectively.

dx.doi.org/10.1021/ic401769s | Inorg. Chem. 2013, 52, 11450−11456

Table 2. Selected Bond Distances (Å) for α-$ScVSe_2O_8$, β-$ScVSe_2O_8$, and $ScVTe_2O_8$

α-$ScVSe_2O_8$		β-$ScVSe_2O_8$		$ScVTe_2O_8$	
V(1)−O(1)	2.005(2)	V(1)−O(1)	2.013(3)	V(1)−O(3)	1.831(7)
V(1)−O(2)	1.933(2)	V(1)−O(1)	2.031(3)	V(1)−O(6)	1.810(7)
V(1)−O(6)	2.145(2)	V(1)−O(2)	1.669(3)	V(1)−O(7)	1.701(8)
V(1)−O(7)	1.642(3)	V(1)−O(3)	1.582(3)	V(1)−O(8)	1.460(13)
V(1)−O(7)	2.249(2)	V(1)−O(4)	1.943(3)		
V(1)−O(8)	1.636(2)			Te(1)−O(1)	1.844(7)
		Se(1)−O(1)	1.798(3)	Te(1)−O(2)	1.916(7)
Se(1)−O(1)	1.753(2)	Se(1)−O(5)	1.669(3)	Te(1)−O(4)	2.075(7)
Se(1)−O(2)	1.699(3)	Se(1)−O(6)	1.664(3)	Te(1)−O(6)	2.209(7)
Se(1)−O(3)	1.665(2)	Se(2)−O(4)	1.684(3)	Te(2)−O(3)	1.916(8)
Se(2)−O(4)	1.681(2)	Se(2)−O(7)	1.689(3)	Te(2)−O(4)	1.914(7)
Se(2)−O(5)	1.678(2)	Se(2)−O(8)	1.695(3)	Te(2)−O(5)	1.878(8)
Se(2)−O(6)	1.726(2)			Te(2)−O(5)	2.508(7)
		Sc(1)−O(2)	2.141(3)		
Sc(1)−O(1)	2.198(2)	Sc(1)−O(5)	2.050(3)	Sc(1)−O(1)	2.021(8)
Sc(1)−O(3)	2.065(2)	Sc(1)−O(6)	2.068(3)	Sc(1)−O(2)	2.150(7)
Sc(1)−O(4)	2.072(2)	Sc(1)−O(7)	2.145(3)	Sc(1)−O(2)	2.166(7)
Sc(1)−O(5)	1.993(3)	Sc(1)−O(7)	2.316(3)	Sc(1)−O(5)	2.081(7)
Sc(1)−O(6)	2.144(2)	Sc(1)−O(8)	2.157(3)	Sc(1)−O(6)	2.147(8)
Sc(1)−O(8)	2.139(2)	Sc(1)−O(8)	2.242(3)	Sc(1)−O(7)	2.100(8)

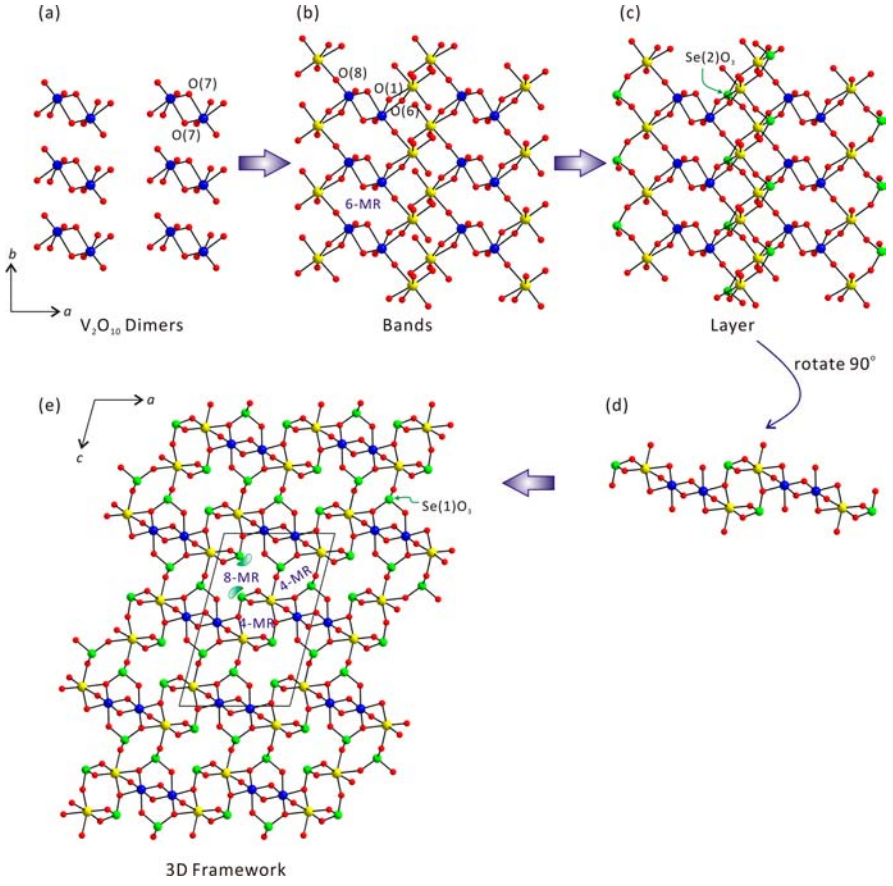

Figure 1. Ball-and-stick representations of α-$ScVSe_2O_8$ (blue, V; green, Se; yellow, Sc; red, O). (a) Two VO_6 octahedra share their edges and form V_2O_{10} dimers. (b) The ScO_6 octahedra share their edges and corners with V_2O_{10} dimers, which generates infinite bands along the [010] direction. (c) A layered structure is obtained by interband linkages of $Se(2)O_3$ groups. (d) Ball-and-stick model of α-$ScVSe_2O_8$ representing one layer in the *ac*-plane. (e) Interlayer linkages by $Se(1)O_3$ groups result in a three-dimensional framework structure.

β-$ScVSe_2O_8$. β-$ScVSe_2O_8$ is another new quaternary mixed metal selenite composed of ScO_7, VO_5, and SeO_3 groups. Although there is no known example for the seven-coordinate Sc^{3+} cation undergoing a SOJT distortion, the Sc^{3+} cations are in distorted pentagonal bipyramidal environment with seven oxygen atoms, in which the lengths for axial Sc−O bonds are shorter (2.050(3)−2.068(3) Å) and those for equatorial Sc−O bonds are slightly longer (2.141(3)−2.316(3) Å). The O−Sc−O

dx.doi.org/10.1021/ic401769s | *Inorg. Chem.* 2013, 52, 11450−11456

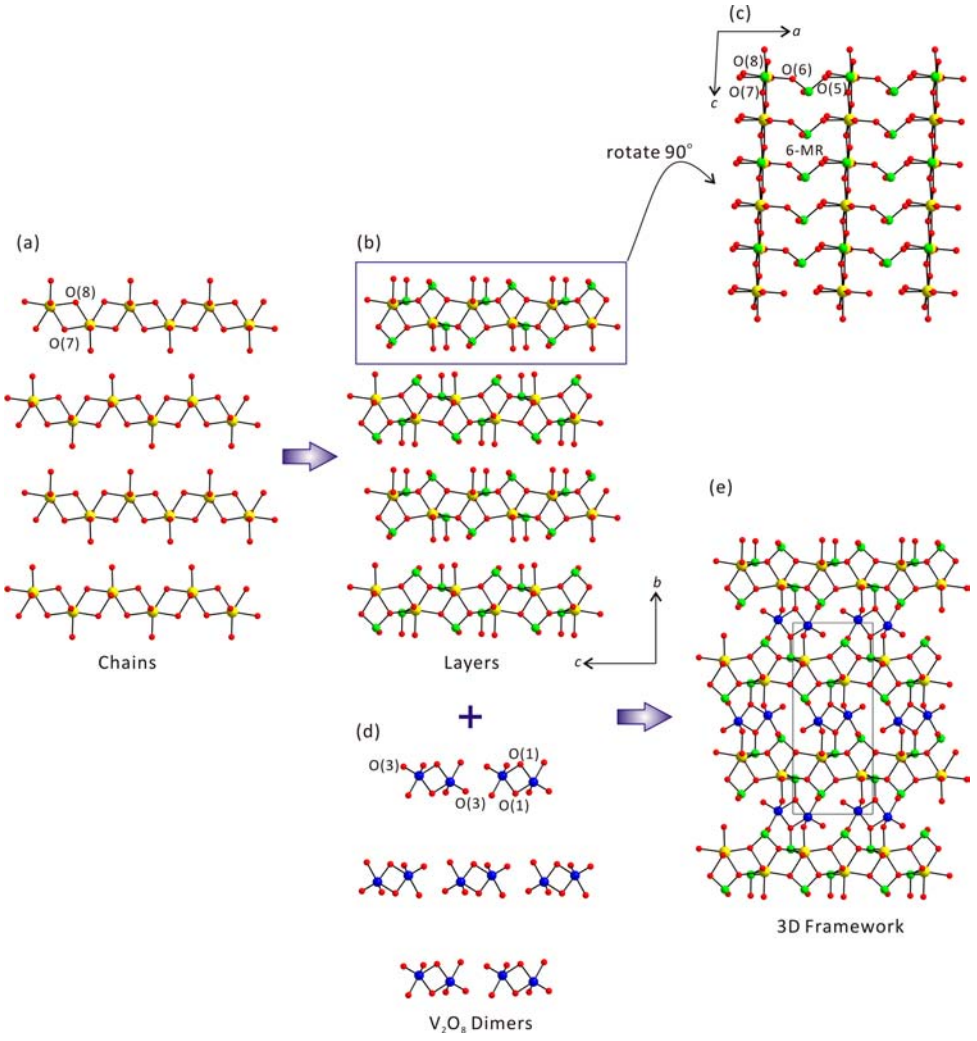

Figure 2. Ball-and-stick representations of β-$ScVSe_2O_8$ (blue, V; green, Se; yellow, Sc; red, O). (a) Each ScO_7 pentagonal bipyramid shares their edges and form infinite chains along the [001] direction. (b) SeO_3 polyhedra are linked to the chains, which generates a layered structure in the *ac*-plane (c) Six-membered rings (6-MRs) are observed within the layer. (d) Two VO_5 square pyramids share their edges and form V_2O_8 dimers. (e) The V_2O_8 dimers link the layers and form a three-dimensional framework structure.

bond angles range from 63.91(11) to 174.56(13)°. The coordination environment of V^{5+} is different to that of α-$ScVSe_2O_8$ as well; each V^{5+} cation is bonded to five oxygen atoms in a distorted square pyramidal geometry with the V−O bond lengths ranging from 1.582(3) to 2.031(3) Å and the O−V−O bond angles of 71.44(15)−152.88(14)°. The shortest V−O bond remains terminal, while four of the five oxygen atoms are further bonded to other cations. The two unique Se^{4+} cations, $Se(1)^{4+}$ and $Se(2)^{4+}$, are bonded to three oxygen atoms in distorted trigonal pyramidal environments. The Se−O bond distances and the O−Se−O bond angles range over 1.664(3)−1.798(3) Å and 91.00(15)−101.08(15)°, respectively.

Each ScO_7 pentagonal bipyramid shares their edges through O(7) and O(8) and form infinite chains along the [001] direction (see Figure 2a). Similar infinite chains of edge-shared pentagonal bipyramids have been observed before from a scandium selenite and a uranyl oxide fluoride.[17] $Se(1)O_3$ and $Se(2)O_3$ polyhedra are linked to the chains through O(5), O(6), O(7), and O(8), which generates a layered structure in the *ac*-plane (see Figure 2b and c). One can notice that the $Se(1)O_3$ and $Se(2)O_3$ groups serve as inter- and intrachain linkers, respectively. Within the layer, six-membered rings (6-MRs) composed of two Se^{4+} and four Sc^{3+} cations are observed. Meanwhile, as seen in Figure 2d, two VO_5 square pyramids share their edges through O(1) and form V_2O_8 dimers, in which the two apical oxygen atoms [O(3)] point toward opposite directions. Finally, the V_2O_8 dimers link the layers, bonding to oxygen atoms in adjacent layers along the [010] direction and form a three-dimensional framework structure (see Figure 2e). In connectivity terms, the structure of β-$ScVSe_2O_8$ can be described as a neutral framework of $\{[ScO_{3/2}\ O_{4/3}]^{-2.667}\ [VO_{1/1}O_{2/2}O_{2/3}]^{-0.333}\ [Se(1)O_{2/2}O_{1/3}]^{+1.333}\ [Se(2)\text{-}O_{1/2}O_{2/3}]^{+1.667}\}^0$. Bond valence calculations[16] for the Sc^{3+}, V^{5+}, Se^{4+}, and O^{2-} result in values of 3.10, 5.05, 3.99−4.17, and 1.82−2.15, respectively.

$ScVTe_2O_8$. Another new quaternary Sc^{3+}−V^{5+}−Te^{4+}−oxide, $ScVTe_2O_8$ exhibits a similar structure to that of $InVTe_2O_8$.[10c] The structure is composed of ScO_6 octahedra, VO_4 tetrahedra, and asymmetric TeO_4 polyhedra that are connected through oxygen atoms. The Sc^{3+} cations are in a distorted octahedral coordination environment, bound to six oxygen atoms with the Sc−O bond distances ranging from 2.021(8) to 2.166(7) Å. The observed O−Sc−O bond angles range from 75.5(3) to 176.3(3)°. The V^{5+} cations are in severely distorted tetrahedral

dx.doi.org/10.1021/ic401769s | *Inorg. Chem.* 2013, 52, 11450−11456

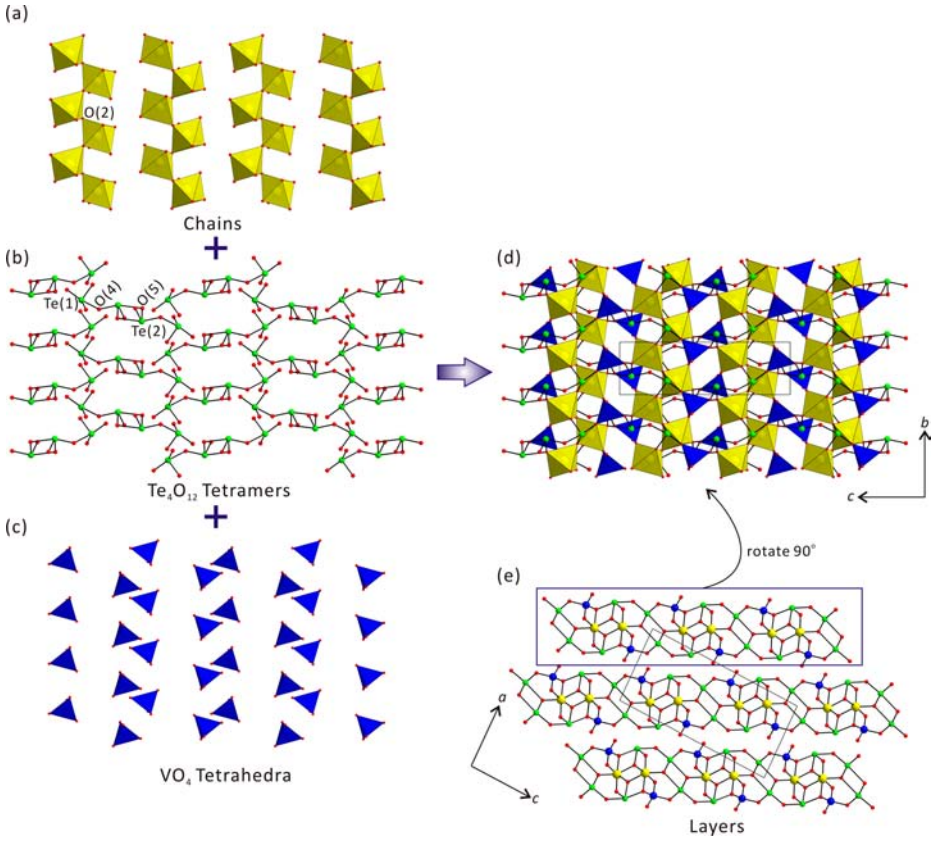

Figure 3. Ball-and-stick and polyhedral diagrams representing (a) chains of corner-shared ScO_6 octahedra along the [010] direction, (b) Te_4O_{12} tetramers, (c) VO_4 tetrahedra, and the linking of the polyhedra to generate a layered structure of $ScVTe_2O_8$ in the (d) *bc*-plane and (e) *ac*-plane (blue, V; green, Te; yellow, Sc; red, O).

coordination environment with the V−O bond lengths and the O−V−O bond angles ranging 1.460(13)−1.831(7) Å and 107.0(3)−114.5(5)°, respectively. The significantly short length of V(1)−O(8) bond exhibits a feature for terminal dioxovanadium(V) (V═O). The two unique Te^{4+} cations are bonded to four oxygen atoms in distorted seesaw environment. While the $Te(1)^{4+}$ cations reveal two slightly shorter (1.884(7) and 1.916(7) Å) and two slightly longer (2.075(7) and 2.209(7) Å) Te−O bond distances, $Te(2)^{4+}$ cations exhibit three shorter (1.878(8)−1.916(8) Å) and one very long (2.508(7) Å) Te−O bond lengths. However, both Te^{4+} cations are in an asymmetric coordination environment attributable to their stereoactive lone pairs. The O−Te−O bond angles range from 71.3(3) to 162.9(3)°.

The ScO_6 octahedra share their corners through O(2) and form infinite zigzag chains along the [010] direction (see Figure 3a). Also, the $Te(1)O_4$ and $Te(2)O_4$ polyhedra share their corners through O(4) and form Te_2O_7 dimers. And then the dimers further share their edges through O(5) and generate Te_4O_{12} tetramers (see Figure 3b). The zigzag chains of corner-shared ScO_6 octahedra, the Te_4O_{12} tetramers, and the VO_4 tetrahedra link together and form the layered structure of $ScVTe_2O_8$ (see Figure 3). In connectivity terms, the structure can be written as neutral layers of $\{[ScO_{2/3}O_{4/3}]^{-1.667}[VO_{1/1}O_{2/2}O_{1/3}]^{+0.333}\ 2[TeO_{2/2}O_{2/3}]^{+0.667}\}^0$. Bond valence calculations[16] for the Sc^{3+}, V^{5+}, Te^{4+}, and O^{2-} result in values of 2.96, 5.19, 3.74−3.80, and 1.76−2.12, respectively.

Infrared Spectroscopy. V−O, Se−O (or Te−O), and Sc−O vibrations are observed in the infrared spectra of α-$ScVSe_2O_8$, β-$ScVSe_2O_8$, and $ScVTe_2O_8$. All three materials reveal the presence of short V═O vibrations in the region of about 907−993 cm^{-1} and V−O vibrations in the region of about 737−873 cm^{-1}. Multiple bands between 408−660 cm^{-1} and 536−788 cm^{-1} are attributed to Se−O and Te−O vibrations, respectively. Bands for Sc−O vibrations are observed around 434−485 cm^{-1}. The assignments are consistent with those previously reported.[10b,18] The infrared spectra for the reported materials have been deposited in the Supporting Information.

Thermogravimetric Analysis. α-$ScVSe_2O_8$ and β-$ScVSe_2O_8$ are only stable up to 460 and 470 °C, respectively. Above these temperatures, decomposition occurs for both compounds attributed to the sublimation of SeO_2. Thermal decomposition products at 1000 °C in air for α-$ScVSe_2O_8$ and β-$ScVSe_2O_8$ resulted in $ScVO_4$[19] as confirmed by powder XRD measurements. With $ScVTe_2O_8$, no weight loss is observed up to 1000 °C. However, an endothermic peak is observed in the heating curve of the differential thermal analysis curve at 750 °C, which indicates the material melts incongruently at the temperature. To confirm the result, powder XRD patterns were measured at higher temperatures. Although no substantial changes in the peak intensities are observed up to 750 °C, the XRD patterns obtained at 800 and 1000 °C are identified as Sc_2TeO_6[20] and some amorphous phases. The TGA data have been deposited in the Supporting Information.

Dipole Moment and Out-of-Center Distortions Calculations. Although all three reported materials crystallize in centrosymmetric space groups, the materials contain lone pair cations (Se^{4+} and Te^{4+}) exhibiting local asymmetric coordination environment. The magnitude and direction of the distortions in the SeO_3 and TeO_4 polyhedra could be quantified by

dx.doi.org/10.1021/ic401769s | *Inorg. Chem.* 2013, 52, 11450−11456

determining the local dipole moments. This approach has been described earlier with respect to octahedra for metal oxyfluorides using bond valence sum calculations.[21] With the lone pair polyhedra, the lone pair is given a charge of −2 and the localized Se^{4+}−lone pair and Te^{4+}−lone pair distances are estimated to be 1.22 and 1.25 Å, respectively, based on the earlier work of Galy et al.[22] Using this methodology, the local dipole moments for the SeO_3 and TeO_4 polyhedra in the reported materials range about 7.61−9.53 D and 9.37−11.06 (D = Debyes), respectively. The values are consistent with those reported dipole moments for SeO_3 and TeO_4 polyhedra.[6i,23] A complete calculation of dipole moments is listed in Table 3.

Table 3. Calculation of Dipole Moments for SeO_3 and TeO_4 Polyhedra[a]

compound	SeO_3 or TeO_4	dipole moment (D)
α-$ScVSe_2O_8$	$Se(1)O_3$	7.61
	$Se(2)O_3$	7.72
β-$ScVSe_2O_8$	$Se(1)O_3$	9.53
	$Se(2)O_3$	7.63
$ScVTe_2O_8$	$Te(1)O_4$	9.37
	$Te(2)O_4$	11.06

[a]D = Debyes.

The magnitude of out-of-center distortions (Δ_d) for VO_6 and ScO_6 octahedra can be quantified. The method takes into account the six M−O bond distances as well as deviations from 180° of the three *trans* O−M−O bond angles.[3b] Using this method, Δ_d for VO_6 octahedra in α-$ScVSe_2O_8$ is calculated to be 1.24, which is greater than the average magnitude of the intraoctahedral distortion scale of 1.10 for V^{5+}. However, calculated Δ_d values for ScO_6 octahedra in α-$ScVSe_2O_8$ and $ScVTe_2O_8$ are 0.36 and 0.27, respectively, which are classified as weak distorters.

Transformation Reactions. The polymorphic characteristics of α-$ScVSe_2O_8$ and β-$ScVSe_2O_8$ suggested that the materials may undergo transformation reactions. Approximately 100 mg of α-$ScVSe_2O_8$ and β-$ScVSe_2O_8$ were heated with 10 mL of water for 4 days under hydrothermal conditions at 230 °C in autoclaves. The reaction products for both reactions turned out to be $Sc_2(SeO_3)_3{\cdot}H_2O$[17a] based on the powder XRD patterns. Interestingly, $Sc_2(SeO_3)_3{\cdot}H_2O$ shares very similar structural features with β-$ScVSe_2O_8$, which includes infinite chains of edge-shared ScO_7 pentagonal bipyramids, intrachain SeO_3 linkers, and interchain SeO_3 linkers. Thus, we can speculate that α-$ScVSe_2O_8$ initially transforms to β-$ScVSe_2O_8$, and then further reactions with water results in the formation of $Sc_2(SeO_3)_3{\cdot}H_2O$ by losing V^{5+} under hydrothermal conditions (see Figure 4). The powder XRD patterns on the resultant reaction products with the generated pattern of $Sc_2(SeO_3)_3{\cdot}H_2O$ from the single-crystal data have been deposited in the Supporting Information.

CONCLUSIONS

A series of new quaternary scandium vanadium selenium/tellurium oxides materials, α-$ScVSe_2O_8$, β-$ScVSe_2O_8$, and $ScVTe_2O_8$ have been successfully synthesized by standard solid-state and/or hydrothermal reactions. All of the constituent cations in the reported materials are in a distorted coordination environment attributed to SOJT effects. All three stoichiometrically equivalent materials exhibit different structures. Crystallographic data indicate that α-$ScVSe_2O_8$ possesses a three-dimensional framework structure composed of ScO_6 octahedra, VO_6 octahedra, and SeO_3 polyhedra. β-$ScVSe_2O_8$ shows another three-dimensional framework with ScO_7 pentagonal bipyramids, VO_5 square pyramids, and SeO_3 polyhedra. However, $ScVTe_2O_8$ reveals a two-dimensional layered structure with ScO_6 octahedra, VO_4 tetrahedra, and TeO_4 polyhedra. Infrared spectroscopy, thermal analyses, dipole moment calculations, and out-of-center distortion calculations have been performed for the reported materials. Transformation reactions indicate that α-$ScVSe_2O_8$ may change to β-$ScVSe_2O_8$, and then to $Sc_2(SeO_3)_3{\cdot}H_2O$ under hydrothermal conditions.

ASSOCIATED CONTENT

Supporting Information

X-ray crystallographic file in CIF format, calculated and observed XRD patterns, thermogravimetric analysis diagrams, and infrared spectra for α-$ScVSe_2O_8$, β-$ScVSe_2O_8$, and $ScVTe_2O_8$. This material is available free of charge via the Internet at http://pubs.acs.org.

AUTHOR INFORMATION

Corresponding Author

*E-mail: kmok@cau.ac.kr. Phone: +82-2-820-5197. Fax: +82-2-825-4736.

Notes

The authors declare no competing financial interest.

ACKNOWLEDGMENTS

This research was supported by Basic Science Research Program through the National Research Foundation of Korea (NRF) funded by the Ministry of Education, Science & Technology (Grant 2013R1A2A2A01007170).

REFERENCES

(1) (a) Nye, J. F. *Physical Properties of Crystals*; Oxford University Press: Oxford, U.K., 1957; (b) Jona, F.; Shirane, G. *Ferroelectric Crystals*;

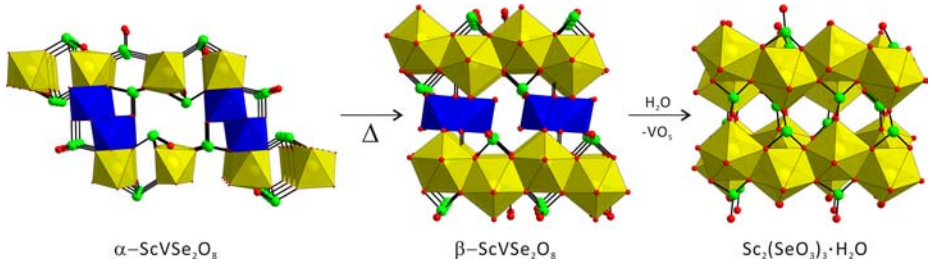

Figure 4. α-$ScVSe_2O_8$ transforms to β-$ScVSe_2O_8$, and then further reactions with water results in the formation of $Sc_2(SeO_3)_3{\cdot}H_2O$ by losing V^{5+} under hydrothermal reaction conditions.

Pergamon Press: Oxford, U.K., 1962; (c) Cady, W. G. *Piezoelectricity; an Introduction to the Theory and Applications of Electromechanical Phenomena in Crystals*; Dover: New York, 1964; (d) Lang, S. B. *Sourcebook of Pyroelectricity*; Gordon & Breach Science: London, U.K., 1974.

(2) (a) Opik, U.; Pryce, M. H. L. *Proc. R. Soc. London* **1957**, *A238*, 425. (b) Bader, R. F. W. *Can. J. Chem.* **1962**, *40*, 1164. (c) Pearson, R. G. *J. Am. Chem. Soc.* **1969**, *91*, 4947. (d) Pearson, R. G. *J. Mol. Struct.: THEOCHEM* **1983**, *103*, 25. (e) Wheeler, R. A.; Whangbo, M.-H.; Hughbanks, T.; Hoffmann, R.; Burdett, J. K.; Albright, T. A. *J. Am. Chem. Soc.* **1986**, *108*, 2222. (f) Kunz, M.; Brown, I. D. *J. Solid State Chem.* **1995**, *115*, 395.

(3) (a) Halasyamani, P. S.; Poeppelmeier, K. R. *Chem. Mater.* **1998**, *10*, 2753. (b) Halasyamani, P. S. *Chem. Mater.* **2004**, *16*, 3586.

(4) (a) Sidgwick, N. V.; Powell, H. M. *Proc. R. Soc. London* **1940**, *A176*, 153. (b) Gillespie, R. J.; Nyholm, R. S. *Q. Rev., Chem. Soc.* **1957**, *11*, 339. (c) Orgel, L. E. *J. Chem. Soc.* **1959**, 3815.

(5) (a) Lefebvre, I.; Lannoo, M.; Allan, G.; Ibanez, A.; Fourcade, J.; Jumas, J. C. *Phys. Rev. Lett.* **1987**, *59*, 2471. (b) Lefebvre, I.; Szymanski, M. A.; Olivier-Fourcade, J.; Jumas, J. C. *Phys. Rev. B* **1998**, *58*, 1896. (c) Watson, G. W.; Parker, S. C. *J. Phys. Chem. B* **1999**, *103*, 1258. (d) Watson, G. W.; Parker, S. C.; Kresse, G. *Phys. Rev. B* **1999**, *59*, 8481. (e) Seshadri, R.; Hill, N. A. *Chem. Mater.* **2001**, *13*, 2892. (f) Waghmare, U. V.; Spaldin, N. A.; Kandpal, H. C.; Seshadri, R. *Phys. Rev. B* **2003**, *67*, 125111. (g) Walsh, A.; Payne, D. J.; Egdell, R. G.; Watson, G. W. *Chem. Soc. Rev.* **2011**, *40*, 4455.

(6) (a) Sykora, R. E.; Ok, K. M.; Halasyamani, P. S.; Albrecht-Schmitt, T. E. *J. Am. Chem. Soc.* **2002**, *124*, 1951. (b) Sykora, R. E.; Ok, K. M.; Halasyamani, P. S.; Wells, D. M.; Albrecht-Schmitt, T. E. *Chem. Mater.* **2002**, *14*, 2741. (c) Ok, K. M.; Orzechowski, J.; Halasyamani, P. S. *Inorg. Chem.* **2004**, *43*, 964. (d) Chen, X. A.; Zhang, L.; Chang, X.; Xue, H.; Zang, H.; Xiao, W. Q.; Song, X.; Yan, H. *J. Alloys Compd.* **2007**, *428*, 54. (e) Ling, J.; Albrecht Schmitt, T. E. *J. Solid State Chem.* **2007**, *180*, 1601. (f) Chang, H. Y.; Kim, S.-H.; Halasyamani, P. S.; Ok, K. M. *J. Am. Chem. Soc.* **2009**, *131*, 2426. (g) Kong, F.; Hu, C.; Hu, T.; Zhou, Y.; Mao, J. G. *Dalton Trans.* **2009**, *2009*, 4962. (h) Yang, B.; Hu, C.; Xu, X.; Sun, C.; Zhang Jian, H.; Mao, J. G. *Chem. Mater.* **2010**, *22*, 1545. (i) Oh, S.-J.; Lee, D. W.; Ok, K. M. *Inorg. Chem.* **2012**, *51*, 5393. (j) Oh, S.-J.; Lee, D. W.; Ok, K. M. *Dalton Trans.* **2012**, *41*, 2995.

(7) (a) Kwon, Y. U.; Lee, K. S.; Kim, Y. H. *Inorg. Chem.* **1996**, *35*, 1161. (b) Hong, Y. S.; Zakhour, M.; Subramanian, M. A.; Darrieta, J. *J. Mater. Chem.* **1998**, *8*, 1889. (c) Harrison, W. T. A. *Acta Crystallogr.* **2000**, *C10*, E422. (d) Harrison, W. T. A.; Buttery, J. H. N. *Z. Anorg. Allg. Chem.* **2000**, *626*, 867. (e) Rozier, P.; Vendier, L.; Galy, J. *Acta Crystallogr.* **2002**, *C58*, i111. (f) Johnston, M. G.; Harrison, W. T. A. *Acta Crystallogr.* **2007**, *C63*, i57. (g) Chang, H. Y.; Kim, S.-H.; Ok, K. M.; Halasyamani, P. S. *Chem. Mater.* **2009**, *21*, 1654.

(8) (a) Hou, J. Y.; Huang, C. C.; Zhang, H. H.; Yang, Q. Y.; Chen, Y. P.; Xu, J. F. *Acta Crystallogr.* **2005**, *C61*, i59. (b) Sivakumar, T.; Ok, K. M.; Halasyamani, P. S. *Inorg. Chem.* **2006**, *45*, 3602. (c) Zhang, S.-Y.; Hu, C.-L.; Sun, C.-F.; Mao, J.-G. *Inorg. Chem.* **2010**, *49*, 11627. (d) Yeon, J. H.; Kim, S. H.; Nguyen, S. D.; Lee, H. N.; Halasyamani, P. S. *Inorg. Chem.* **2012**, *51*, 609.

(9) (a) Feger, C. R.; Kolis, J. W. *Acta Crystallogr.* **1998**, *C54*, 1217. (b) Millet, P.; Enjalbert, R.; Galy, J. *J. Solid State Chem.* **1999**, *147*, 296. (c) Jiang, H.; Huang, S.; Fan, Y.; Mao, J.; Cheng, W. *Chem.—Eur. J.* **2008**, *14*, 1972. (d) Jiang, H.; Kong, F.; Fan, Y.; Mao, J. G. *Inorg. Chem.* **2008**, *47*, 7430. (e) Zhang, D.; Johnsson, M. *Acta Crystallogr.* **2009**, *C65*, i9. (f) Rabbani, F.; Zimmermann, I.; Johnsson, M. *Acta Crystallogr.* **2012**, *E68*, i61.

(10) (a) Li, P. X.; Kong, F.; Hu, C. L.; Zhao, N.; Mao, J. G. *Inorg. Chem.* **2010**, *49*, 5943. (b) Li, P.-X.; Zhang, S.-Y.; Mao, J.-G. *Dalton Trans.* **2010**, *39*, 11560. (c) Lee, D. W.; Oh, S. J.; Halasyamani, P. S.; Ok, K. M. *Inorg. Chem.* **2011**, *50*, 4473.

(11) *SAINT, Program for Area Detector Absorption Correction*, version 4.05; Siemens Analytical X-ray Instruments: Madison, WI, 1995.

(12) Blessing, R. H. *Acta Crystallogr., Sect. A: Found. Crystallogr.* **1995**, *A51*, 33.

(13) Sheldrick, G. M.; *SHELXS-97 - A program for automatic solution of crystal structures*; University of Goettingen: Goettingen, Germany, 1997.

(14) Sheldrick, G. M.; *SHELXL-97 - A program for crystal structure refinement*; University of Goettingen: Goettingen, Germany, 1997.

(15) Farrugia, L. J. *J. Appl. Crystallogr.* **1999**, *32*, 837.

(16) (a) Brown, I. D.; Altermatt, D. *Acta Crystallogr.* **1985**, *B41*, 244. (b) Brese, N. E.; O'Keeffe, M. *Acta Crystallogr.* **1991**, *B47*, 192.

(17) (a) Johnston, M. G.; Harrison, W. T. A. *J. Solid State Chem.* **2004**, *177*, 4316. (b) Ok, K. M.; Doran, M. B.; O'Hare, D. *J. Mater. Chem.* **2006**, *16*, 3366.

(18) (a) Hewston, T. A.; Chamberland, B. L. *J. Phys. Chem. Solids* **1987**, *48*, 97. (b) Akama, Y.; Sawada, T.; Ueda, T. *J. Mol. Struct.* **2005**, *750*, 44. (c) Kim, M. K.; Kim, S.-H.; Chang, H.-Y.; Halasyamani, P. S.; Ok, K. M. *Inorg. Chem.* **2010**, *49*, 7028.

(19) Cong, H.; Zhang, H.; Yao, B.; Yu, W.; Zhao, X.; Wang, J.; Zhang, G. *Cryst. Growth Des.* **2010**, *10*, 4389.

(20) Höss, P.; Schleid, T. *Z. Anorg. Allg. Chem.* **2007**, *633*, 1391.

(21) (a) Maggard, P. A.; Nault, T. S.; Stern, C. L.; Poeppelmeier, K. R. *J. Solid State Chem.* **2003**, *175*, 25. (b) Izumi, H. K.; Kirsch, J. E.; Stern, C. L.; Poeppelmeier, K. R. *Inorg. Chem.* **2005**, *44*, 884.

(22) Galy, J.; Meunier, G. *J. Solid State Chem.* **1975**, *13*, 142.

(23) (a) Ok, K. M.; Halasyamani, P. S. *Inorg. Chem.* **2005**, *44*, 3919. (b) Kim, M. K.; Jo, V.; Lee, D. W.; Ok, K. M. *Dalton Trans.* **2010**, *39*, 6037. (c) Lee, D. W.; Ok, K. M. *Solid State Sci.* **2010**, *12*, 2036. (d) Lee, D. W.; Bak, D.-b.; Kim, S. B.; Kim, J.; Ok, K. M. *Inorg. Chem.* **2012**, *51*, 7844. (e) Lee, D. W.; Kim, S. B.; Ok, K. M. *Inorg. Chem.* **2012**, *51*, 8530. (f) Lee, D. W.; Ok, K. M. *Inorg. Chem.* **2013**, *52*, 5176.